HHS Public Access

Author manuscript

J Physiol. Author manuscript; available in PMC 2023 November 01.

Published in final edited form as:

J Physiol. 2022 November ; 600(21): 4695–4711. doi:10.1113/JP283318.

Bile acids regulate the epithelial Na^+ channel in native tissues through direct binding at multiple sites

Xue-Ping Wang[1], **Viktor Tomilin**[2], **Andrew J. Nickerson**[1], **Runze Tian**[3], **Merve Ertem**[1], **Abagail McKernan**[1], **Xiaoguang Lei**[3], **Oleh Pochynyuk**[2], **Ossama B. Kashlan**[1,4]

[1]Department of Medicine, Renal-electrolyte Division, University of Pittsburgh, Pittsburgh, Pennsylvania

[2]Department of Integrative Biology and Pharmacology, University of Texas Health Science Center at Houston, Houston, Texas

[3]Beijing National Laboratory for Molecular Sciences, Department of Chemical Biology, College of Chemistry and Molecular Engineering, and Peking-Tsinghua Center for Life Sciences, Peking University, Beijing, China

[4]Department of Computational and Systems Biology, University of Pittsburgh, Pittsburgh, Pennsylvania

Abstract

Bile acids, originally known to emulsify dietary lipids, are now established signaling molecules that regulate physiological processes. Signaling targets several proteins that include ion channels involved in regulating intestinal motility and bile viscosity. Studies show that bile acids regulate the epithelial sodium channel (ENaC) in cultured cell models and heterologous expression systems. ENaC plays both local and systemic roles in regulating extracellular fluids. Here we investigated whether bile acids regulate ENaC expressed in native tissues. We found that taurocholic acid and taurohyodeoxycholic acid regulated ENaC in both the distal nephron and distal colon. We also tested the hypothesis that regulation occurs through direct binding. Using photoaffinity labeling, we found evidence for specific binding to both the β and γ subunits of the channel. In functional experiments, we found that the α subunit was sufficient for regulation. We also found that regulation by at least one bile acid was voltage-sensitive, suggesting that one binding site may be closely associated with the pore-forming helices of the channel. Our data provide evidence that bile acids regulate ENaC by binding to multiple sites to influence the open probability of the channel.

To whom correspondence should be addressed: Ossama Kashlan, Department of Medicine, Renal-Electrolyte Division, University of Pittsburgh, S828B Scaife Hall, 3550 Terrace St., Pittsburgh, Pennsylvania 15261; Telephone: (412)648-9275; obk2@pitt.edu.

Author Contributions

X.P.W., A.N., X.L., O.P. and O.B.K. designed research. X.P.W., V.T., A.N., M.E., R.T. and A.M. performed research. X.P.W., V.T., A.N., M.E., R.T., A.M., O.P. and O.B.K. analyzed the data. X.P.W. and O.B.K. wrote the paper. All authors revised the paper and approved the final version of the manuscript. All authors agree to be accountable for all aspects of the work in ensuring that questions related to the accuracy or integrity of any part of the work are appropriately investigated and resolved. All persons designated as authors qualify for authorship, and all those who qualify for authorship are listed.

Competing Interests

The authors declare no conflicts of interest.

Graphical Abstract

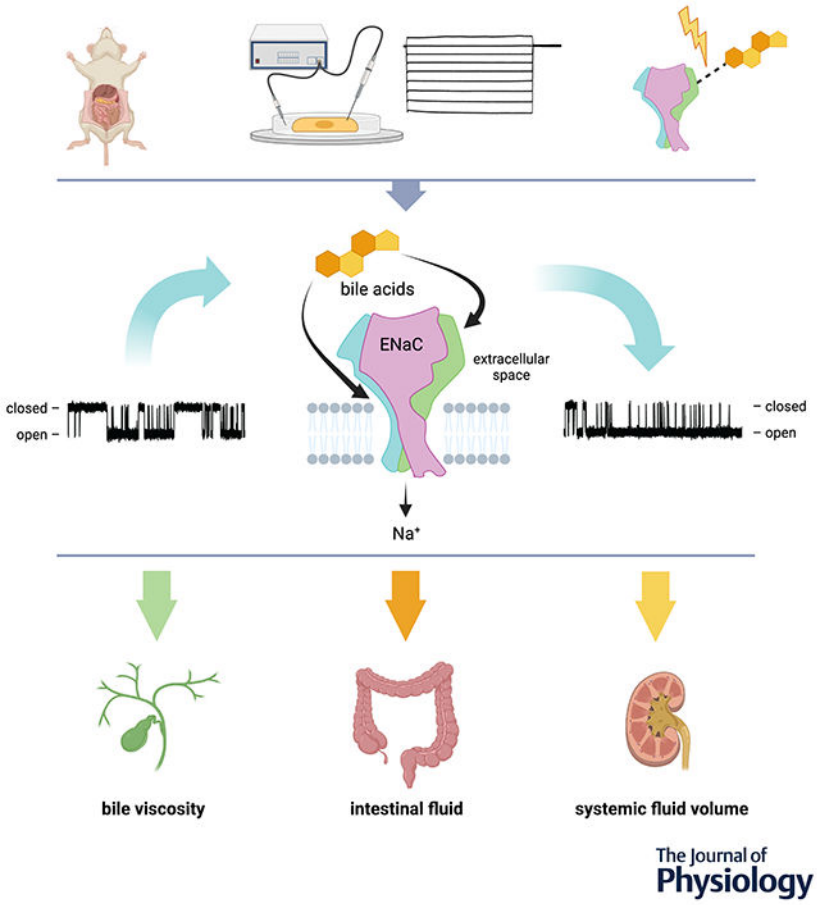

ENaC regulation by bile acids was investigated using native mouse tissues, heterologous expression systems, electrophysiological approaches, and photoaffinity labeling. We found that bile acids directly bind the channel and regulate activity by changing the probability that the channel is open and conducting Na^+. Functional data and photoaffinity labeling experiments provide evidence for multiple binding sites involving more than one ENaC subunit. Voltage-dependent data support at least one site binding associated with the voltage-gradient of the cell membrane. We conclude that bile acids are ENaC effectors that may influence the physiology of the biliary tree, distal colon, or distal nephron in normal or diseased states.

Keywords

mouse ENaC; allostery; taurocholic acid; photoaffinity labeling; patch clamp; Ussing chamber; amiloride

Introduction

Bile acids, the major organic component of bile, both emulsify dietary fats and regulate protein function. High concentrations of bile acids are generally confined to the

enterohepatic circulation, but are markedly elevated in the blood and urine of advanced liver disease patients (Miura et al., 2011; Brandl et al., 2018). In addition to signaling through bile acid receptors, bile acids regulate ion channels on luminal surfaces that have a role in regulating fluid composition and volume (Keely et al., 2022). Cholangiocytes, colonocytes, endothelial cells, and renal principal cells express the epithelial Na^+ channel (ENaC), and growing evidence suggests that bile acids have a role in regulating ENaC function.

ENaC provides for electrogenic Na^+ transport across the apical membranes of several epithelia. The activity of the channel in cholangiocytes and colonocytes regulates bile viscosity and fecal fluid content, respectively (Zeissig et al., 2008; Li et al., 2016). In the kidney, ENaC maintains whole-body Na^+, K^+ and extracellular fluid volume homeostasis (Pearce et al., 2015). Consequently, abnormal ENaC function can result in significant fluid and electrolyte imbalances (Rotin & Staub, 2021). Classical channels are heterotrimers comprising paralogous α, β and γ subunits that have two transmembrane helices, intracellular amino and carboxyl-termini, and large extracellular regions with homologous folds (Figure 1B) (Noreng et al., 2018). Noncanonical trimeric assemblies form when specific subunits are absent (Canessa et al., 1994; Stewart et al., 2011).

We reported that bile acid regulation of ENaC depends on the position and stereochemistry of specific bile acid functional groups (Figure 1A) (Wang et al., 2019). Physico-chemical properties did not correlate with effects on ENaC currents, in line with another study examining ENaC regulation by amphipathic compounds (Schmidt et al., 2018). Bile acids activate ENaC *in vitro* by increasing channel open probability (P_o) (Wiemuth et al., 2014; Ilyaskin et al., 2016; Wang et al., 2019). Regulation through either membrane effects or specific interaction have been proposed (Ilyaskin et al., 2016; Schmidt et al., 2018). How bile acids regulate ENaC remains poorly understood, including whether bile acids regulate ENaC in native tissues, whether they bind the channel directly, and if so, where those physical interactions may occur.

Here we investigated the mechanism of action under the hypothesis that bile acids directly bind ENaC and allosterically regulate its function. We found that bile acids regulate ENaC in native tissues by modulating P_o. Experiments examining the influence of voltage showed that regulation was voltage-sensitive for taurocholic acid (t-CA), but not for taurohyodeoxycholic acid (t-HDCA). Modeling of voltage-sensitive data supports the presence of multiple binding sites. We used functional and crosslinking approaches to determine which subunits hosted bile acid binding sites. Experiments with functional channels lacking specific subunits showed that the α subunit was sufficient to sense bile acids. Photoaffinity labeling experiments using a derivatized bile acid showed specific crosslinking to both the β and γ subunits. Our data provide evidence for an allosteric model of ENaC regulation by bile acids, characterized by multiple binding sites involving all three subunits and effects determined by affinities for various sites.

Methods

Ethical Approval–

Animal work was performed at the University of Pittsburgh and the University of Texas Health Science Center at Houston in conditions compliant with institutional requirements, the National Institutes of Health (NIH), and the American Veterinary Medicine Association (AVMA). All performed procedures were approved under University of Pittsburgh Animal Care and Use Committee protocol nos 20128471 and 21018704 and University of Texas Health Science Center at Houston Animal Care and Use Committee protocol no AWC-19-0056. All animals had free access to food and water. Details of anesthetic administration and euthanasia are detailed below. All authors understood the ethical principles that The Journal of Physiology operates under, and the work complied with the animal ethics checklist reported by Grundy (Grundy, 2015).

Materials–

Bile acids were obtained from commercial sources: DCA (Sigma-Aldrich, Maryland Heights, MO), t-CA and t-DCA (Cayman Chemical, Ann Arbor, MI), and t-HDCA (Spectrum Chemical, New Brunswick, NJ). DCA-p was synthesized as previously described (Zhuang et al., 2017). cDNAs encoding wild type mouse α, β and γ ENaC subunits were cloned in pBluescript SK(−) (Stratagene, San Diego, CA) (Ahn et al., 1999). Corresponding cRNAs for *Xenopus* oocyte injection were synthesized using mMESSAGE mMACHINE kits (ThermoFisher). Untagged or C-terminal V5 tagged mouse wild type and mutants ENaC subunits in pcDNA3.1 were previously described (Hughey et al., 2003; Bruns et al., 2007; Carattino et al., 2008). Ser518 of the C-terminal V5 tagged β subunit was mutated to Lys using the Quikchange II XL Site-directed Mutagenesis kit (Agilent, Santa Clara, CA) and confirmed by direct sequencing.

Isolation of split-open renal collecting ducts–

We isolated renal collecting ducts for patch clamp experiments from 6-10 week old C57BL/6J male mice as previously described (Mamenko et al., 2012a; Mamenko et al., 2013; Mironova et al., 2013; Prieto et al., 2017). Briefly, we sacrificed mice using CO_2 followed by exsanguination, after which kidneys were immediately removed. Kidneys slices (<1 mm) were placed into cold physiological saline solution (PSS, pH 7.35, 0 °C) containing 150 mM NaCl, 5 mM KCl, 1 mM $CaCl_2$, 2 mM $MgCl_2$, 5 mM glucose and 10 mM HEPES. We visually identified collecting ducts by their morphological features (pale color, coarse surface, and occasionally, bifurcations) and mechanically isolated them using watchmaker forceps under a stereomicroscope. Isolated tubules were attached to a 5 mm × 5 mm cover glass coated with poly-L-lysine, which was placed in a chamber mounted on an inverted Nikon Eclipse Ti microscope and perfused with PSS at room temperature. Two sharpened micropipettes controlled with different micromanipulators were used to split open tubules to gain access to the apical membrane, which were used within 2 h of isolation.

Patch clamp current measurement in split-open collecting ducts–

ENaC currents in principal cells were measured in cell-attached patches on the apical membrane under voltage-clamp conditions ($-V_p = -60$ mV) as previously described (Mamenko et al., 2012a; Mamenko et al., 2012b; Mamenko et al., 2013; Prieto et al., 2017). We recorded currents using pipettes with a resistance of 8-10 MΩ in a permanently perfused bath (1.5 ml/min). Bath solution was 150 mM NaCl, 5 mM KCl, 1 mM $CaCl_2$, 2 mM $MgCl_2$, 5 mM glucose and 10 mM HEPES (pH 7.35). The tip of the recording pipette (approximately 3 mm) was filled with control solution containing 140 mM LiCl, 2 mM $MgCl_2$ and 10 mM HEPES (pH 7.35). The rest of pipette was filled by the same solution supplemented with either 1 mM t-CA or 1 mM t-HDCA, as indicated. Gap-free single channel current data from high GΩ seals were acquired and analyzed with Axopatch 200B (Molecular Devices, Sunnyvale, CA) patch clamp amplifier interfaced via a Digidata 1440 (Molecular Devices) to a PC running the pClamp 10.5 suite of software (Molecular Devices). Currents were low-pass filtered at 100 Hz with an eight-pole Bessel filter (Warner Instruments, Hamden, CT). Gating events were inspected visually prior to acceptance. ENaC activity was analyzed over a span of 60–120 s for each experimental condition. As previously described (Mamenko et al., 2012b), we can reliably ($p < 0.05$) estimate the maximal number of functional ENaC in a patch using this time span. Channel activity in individual patches, defined as $N{\cdot}P_o$, was calculated using as follows: $N{\cdot}P_o = (t_1 + 2t_2 + \ldots + nt_n)$, where N and P_o are the number of channels in a patch and the mean open probability of these channels, respectively, and t_n is the fractional open time spent at each of the observed current levels. P_o was calculated by dividing $N{\cdot}P_o$ by the number of active channels within a patch as defined by all-point amplitude histograms. For representation, current traces were corrected for slow baseline drift as necessary.

Measurement of short-circuit currents in distal colon–

We isolated distal colon for short-circuit current (I_{SC}) experiments from 6-8 week old C57BL/6J male mice as previously described (Nickerson et al., 2021). Briefly, mice were fed a low salt diet for 9-10 days prior to surgery. Mice were anesthetized with 5% isoflurane and euthanized via cervical dislocation. Colons were immediately removed and placed in a Sylgard-coated dish containing ice-cold Ringer's solution (140 mM Na^+, 5.2 mM K^+, 1.2 mM Ca^{2+}, 1.2 mM Mg^{2+}, 119.8 mM Cl^-, 25 mM HCO_3^-, 2.4 mM HPO_4^{2-}, 0.4 $H_2PO_4^-$, and 10 glucose, pH 7.41), opened longitudinally along the mesenteric border and pinned mucosal side facing downward. Preparations of late distal colon (1-3 cm from the rectum) were mounted on tissue sliders (0.3 cm^2) in an Ussing-style recording chamber (VCC-MC6, Physiologic Instruments, San Diego, CA). Tissues were bathed bilaterally in Ringer's solution, while gradually warming to 37 °C and bubbling continuously with 5% CO_2, 95% O_2. Each chamber was equipped with separate pairs of voltage-sensing and current-injecting AgCl electrodes connected to the chamber baths via 3 M KCl agar bridges. After mounting, we monitored trans-epithelial potential (V_{TE}) and allowed it to stabilize (~15 min). We then voltage-clamped the tissues and measured I_{SC} continuously via pClamp 10.5 software (Molecular Devices). By convention, positive I_{SC} values reflect cation (Na^+) absorption and/or anion (Cl^-/HCO_3^-) secretion. Transepithelial conductance (G_{TE}) was also monitored throughout the recording by applying a bi-directional 0.5 second, 10 mV pulse at 30 second intervals via an automated pulse generator. Bile acids and amiloride were

prepared as 200x and 1000x stock solutions in water or DMSO, respectively, and added to the bath as indicated.

Xenopus oocyte isolation and heterologous expression–

Oocytes were harvested from adult female *Xenopus Laevis* using protocols approved the University of Pittsburgh's Institutional Animal Care and Use Committee. Briefly, frogs were first anesthetized in 0.15% (w/v) tricaine (MS-222) buffered by bicarbonate (0.2% (w/v)) for 30 min, verified by gentle foot squeeze, and then ovaries were removed. Frogs were then euthanized by immersion in anesthetic solution for 1 hr followed by pithing. Defolliculation was carried out for 1h at room temperature using 2 mg/ml type IV collagenase in Ca^{2+}-free SOS buffer (100 mM NaCl, 2 mM KCl, 5 mM HEPES, pH 7.4, supplemented with and 3 mg/ml Trypsin inhibitor). Defolliculated oocytes were stored at 18 °C in modified Barth's saline (88 mM NaCl, 1 mM KCl, 2.4 mM $NaHCO_3$, 15 mM HEPES, 0.3 mM $Ca(NO_3)_2$, 0.41 mM $CaCl_2$, and 0.82 mM $MgSO_4$, pH 7.4) supplemented with 10 μg/ml of sodium penicillin, 10 μg/ml of streptomycin sulfate, and 100 μg/ml of gentamicin sulfate. 1 ng of cDNA per ENaC subunit was injected into stage V or VI *Xenopus* oocytes using a Nanoject II (Drummond, Broomall, PA).

Whole cell current measurements in Xenopus oocytes–

ENaC current was measured using the two-electrode voltage clamp (TEVC) technique 24 h after cDNA injection. Oocytes were maintained in a 20-μl recording chamber (AutoMate Scientific, Berkeley, CA) and continuously perfused with Na-110 buffer (110 mM NaCl, 2 mM KCl, 2 mM CaCl2, 10 mM HEPES, pH 7.4) at a flow rate of 3-5 ml/min. A final concentration of 1 mM t-CA was diluted into Na-110 buffer from 200 mM stock in water. At the end of each experiment, currents were measured in 10 μM amiloride (100 mM stock solution in dimethyl sulfoxide diluted into Na-110 buffer) to determine the amiloride sensitive component of the current. Voltage clamp was performed using an Axoclamp 900 voltage amplifier (Molecular Devices, Sunnyvale, CA) and DigiData 1440A interface (Molecular Devices). Electrophysiological data were analyzed with Clampfit 10.5 and plotted with Graphpad Prism 7.0.

Curve fitting for voltage-dependent data–

Voltage-dependent dose-response curves were fit using Igor Pro 6 (Wavemetrics). Relative activation as a function of voltage for each bile acid dose was defined as:

$$\Delta I = \frac{[\text{open channels at } [B] = X]_V}{[\text{open channels at } [B] = 0]} - 1 \quad (2)$$

where B is the bile acid. This model assumes that all open-states have the same conductance and that all closed-states have no conductance. Equilibrium constants based on the regulatory model (Figure 5F) assumed independent binding at each site, where O and C are the unbound open and closed states, respectively, and were used to define each state in terms of [O] and [B]:

$$K_o = \frac{[O]}{[C]};\ K_1 = \frac{[O][B]}{[O{-}B1]}\frac{[O{-}B2][B]}{[O{-}B1-B2]}$$

$$K_2 = \frac{[C][B]}{[C{-}B]};\ K_3 = \frac{[O][B]}{[O{-}B2]}\frac{[O{-}B1][B]}{[O{-}B1-B2]}$$

$$[C] = \frac{[O]}{K_o};\ [C{-}B] = \frac{[O][B]}{K_o K_2};\ [O{-}B1] = \frac{[O][B]}{K_1}$$

$$[O{-}B2] = \frac{[O][B]}{K_3};\ [O{-}B1-B2] = \frac{[O][B]^2}{K_1 K_3}$$

We assumed conservation of the total number of channels ($ENaC_T$) during the experiment:

$$\begin{aligned} ENaC_T &= [O] + [C] + [C{-}B] + [O{-}B1] + [O{-}B2] + [O{-}B1-B2] \\ &= [O]\left\{1 + \frac{1}{K_o} + \frac{[B]}{K_o K_2} + \frac{[B]}{K_1} + \frac{[B]}{K_3} + \frac{[B]^2}{K_1 K_3}\right\} \end{aligned} \quad (3)$$

Voltage-dependence for each of the dissociation constants (K_n) was given by eq. 1. Incorporating voltage-dependent dissociation constants and combining equations 2 and 3 gives:

$$\Delta I = \frac{1 + \frac{1}{K_o}}{1 + \frac{1}{K_o} + \frac{[B]}{K_o K_2^V} + \frac{[B]}{K_1^V} + \frac{[B]}{K_3^V} + \frac{[B]^2}{K_1^V K_3^V}} \quad (4)$$

which was used to simulate the data. Fits were performed for all doses simultaneously using the built-in Global Fitting routine in Igor Pro. For model D, there were 7 fitted parameters: K_o, and a K_n and δ_n for each site. Simpler models were fit by restricting specific K_n and δ_n values to ∞ and 0, respectively, removing 2 fitted parameters for each site eliminated. Nested models were compared by F-test. The F statistic was calculated according to

$$F = \frac{\left(\frac{\chi_1^2 - \chi_2^2}{p_2 - p_1}\right)}{\left(\frac{\chi_2^2}{n - p_2}\right)},$$

where χ^2 and p are the residual sum of squares and number of parameters for a given model, respectively, model 2 has the greater number of parameters, and n is the number of fitted

data points. *P* values were calculated using the *fdist* function of Excel, the *F* statistic, and ($p_2 - p_1$, $n - p_2$) degrees of freedom.

FRT cell growth and heterologous expression–

FRT cells were cultured in DMEM/F-12 medium supplemented with 8% fetal bovine serum as previously described (Heidrich et al., 2015). FRT cells were seeded on 6-well plates and transfected with plasmids encoding wild type ENaC subunits (1 μg per subunit), using lipofectamine 3000 according to the manufacturer's protocol. For each construct, only one subunit had a N-terminal HA and C-terminal V5 epitope tags ($^{HA}\alpha^{V5}\beta\gamma$, $\alpha^{HA}\beta^{V5}\gamma$ or $\alpha\beta^{HA}\gamma^{V5}$). Cells were used for bile acid probes crosslinking 24 h after transfection.

UV crosslinking and isolation of labeled proteins–

Transfected cells expressing wild type ENaC were washed with PBS buffer, then incubated with 50 μM bile acid probes diluted in DMEM/F-12 medium at incubator in dark for 1 h. For competition assays, 1 mM tauroconjugated bile acids were co-treated with bile acid probes simultaneously. We irradiated cells at 365 nm for 5 min using a broad-spectrum LED light source (Prixmatix, San Diego, CA) to crosslink the bile acid probes to their bound protein targets. After washing with PBS buffer twice, we extracted cells with 0.2 ml per well of detergent solution supplemented with protease inhibitor Cocktail Set III for 20 min at 4°C and centrifuged for 7 min at 20,000 *g* to remove cell debris. Proteins were quantified using Pierce Rapid Gold BCA Protein Assay Kit (Thermo Fisher) on a microplate reader (Bio-Rad) and normalized to 2 μg/ml. 0.1 ml of each slurry was conjugated with biotin-azide by "click chemistry" in the dark at room temperature for 1 h (100 μM biotin-azide, 100 μM TBTA, 1 mM $CuSO_4$, 1 mM TCEP, and protease inhibitor Cocktail set III). The precipitated proteins were collected and washed with methanol for twice and solubilized with 1.2% SDS/PBS. The solubilized proteins were incubated with anti-V5 tagged streptavidin beads at room temperature for 3 h rotation. After washing the beads with 0.5 ml PBS three times and adding Laemmli sample buffer, the slurry will be heated to 95 °C for 3 min, and the resulting supernatant will be subject to blotting. For biotinylation surface labeling sequential crosslinking, before extracting cells with detergent solution, cells surface proteins were labeled with freshly prepared 1 mg/ml EZ-Link™ Sulfo-NHS-SS-Biotin on ice for half an hour. Excess biotin was quenched by washing with cell culture media twice and cold Dulbecco's PBS buffer twice. Then, proteins in each well were extracted with 0.3 ml detergent solution supplemented with protease inhibitor cocktail set III (Sigma-Aldrich). An aliquot of lysates was saved (5%), and the remaining lysates were incubated with NeutrAvidin beads overnight. The next day, biotin labeled surface proteins were recovered by 50 mM DTT containing solution, 10% of the slurry was retained for surface expression, and the left slurry was subjected for following "Click-chemistry" crosslinking assay directly manipulated as above.

SDS-PAGE and immunoblotting–

Denatured protein samples were subjected to 4%-12% reducing Criterion TGX precast gel (Bio-Rad). Resolved proteins were transferred to 0.45 μm nitrocellulose membrane (Invitrogen) and blocked with 5% nonfat dry milk in PBS for 1 h at room temperature. Membranes were incubated with anti-V5 primary antibodies (1:5000) overnight at 4°C. The

next day, membranes were washed three times with PBS and incubated with horseradish peroxidase-conjugated secondary antibodies (1:5000) at room temperature for 1 h. After washing in PBS, membranes were visualized with Clarity max ECL chemiluminescence kit and ChemiDoc imager (Bio-Rad). Quantitative densitometric analysis was performed using Image Lab (Bio-Rad).

Statistical Analysis–

The results of all individual experiments are presented in the figures. Error bars in dose response curves are S.E.M. All other summary statistics are mean (SD). Statistical tests used are indicated with each figure. Student's t tests, one-way ANOVA and two-way ANOVA were performed using Prism 9.3.1 (GraphPad Software, La Jolla, CA, USA). Curve fitting was performed using IgorPro 6.3 (Wavemetrics, Oswego, OR, USA). Comparison of fits by F-test was performed using Excel 16.60 (Microsoft, Redmond, WA, USA). P values of less than 0.05 were considered significant. All experiments were formed using three or more separate preparations.

Results

Bile acids regulate ENaC in native tissues–

Bile acid regulation of ENaC depends on specific functional groups and does not require bile acids to be membrane permeable (Wang et al., 2019). For example, in *Xenopus* oocytes and cultured collecting duct cells (mpkCCD$_{14}$) membrane impermeant t-CA (3α-OH, 7α-OH, 12α-OH, Figure 1A) activates mouse ENaC and membrane impermeant t-HDCA (3α-OH, 6α-OH, Figure 1A) inhibits mouse ENaC. We hypothesized that bile acids bind ENaC at one or more extracellularly accessible sites and change the channel's P_o. As such a mechanism should be independent of cell type, we determined whether regulation was evident in ENaC expressed in native tissues.

To assess regulation in renal tubules, we performed patch clamp measurements in isolated split open cortical collecting ducts. Mice were fed a normal salt diet (0.32% Na^+) for experiments with t-CA, where we anticipated activation. For experiments with t-HDCA, where we anticipated inhibition, mice were fed a sodium deficient salt diet (<0.01% Na^+) to increase basal P_o (Mamenko et al., 2018). We isolated cortical collecting ducts from mouse kidneys, split them open to access the apical surface, and performed patch clamp experiments in the cell-attached mode (Figures 2A, B). Patch pipettes were backfilled with either 1 mM t-CA or 1 mM t-HDCA. After forming a high GΩ contact, current recordings were started with the pipette potential held at $-V_p = -60$ mV. At the start of each recording, currents were nominally bile acid-free and were used as the control condition. Currents collected after 4 min, allowing for the diffusion of backfilled compounds, were used as the experimental condition. We found that t-CA increased ENaC P_o by 72 (65)%, while t-HDCA decreased ENaC P_o by 54 (46)% (Figure 2C). These results are consistent with t-CA and t-HDCA effects reported previously in cultured cell and *Xenopus* oocyte experiments (Wang et al., 2019).

We next assessed regulation in the distal colon, where ENaC is expressed on the apical membranes of epithelial cells (Garty & Palmer, 1997). ENaC activity was measured as short-circuit current (I_{SC}) in the distal colons of mice. As above, mice were fed a normal salt diet for experiments with t-CA where we anticipated activation, and a sodium deficient diet to increase basal currents (Bertog et al., 2008) for experiments with t-HDCA where we anticipated inhibition. Changes in I_{SC} after bile acid addition were then quantified in the presence and absence of amiloride, an ENaC pore blocker. Consistent with results in the cortical collecting duct, addition of 1 mM t-CA to the apical bath increased I_{SC} (Figures 3A, B) while addition of 1 mM t-HDCA decreased I_{SC} (Figure 3C, D). In both cases, pretreatment with amiloride attenuated the response, consistent with effects on ENaC-mediated currents. We also assessed the effect of 1 mM t-CA on distal colons from mice fed a sodium deficient diet. Although we observed a modest response shortly after adding t-CA in some recordings, the effect was transient (Figures 3E, F). As it was unaltered by the presence of amiloride, it appears that t-CA did not stimulate ENaC under these conditions. This result contrasts with the t-CA effect on ENaC on a normal salt diet (Figures 2C, 3B). We and others previously showed that activating channels through proteolysis precluded activation by bile acids (Wiemuth et al., 2014; Wang et al., 2019). These data hint that aldosterone, stimulated by a low salt diet, may promote ENaC cleavage in the colon, as has been demonstrated in the distal nephron (Carattino et al., 2014; Frindt & Palmer, 2015; Terker et al., 2016; Frindt et al., 2021).

ENaC response to t-CA varies with subunit composition–

To determine whether subunit composition affects ENaC sensitivity to bile acids, we tested the effect of 1 mM t-CA on functional subunit combinations. Robust amiloride-sensitive currents are readily detected upon co-expression of mouse ENaC α, β, and γ subunits (αβγ) in *Xenopus* oocytes. Smaller amiloride-sensitive currents are detected when the α subunit is expressed alone (α_3) or in tandem with β (αβ) or γ (αγ) subunits (Canessa et al., 1994). As ENaC is Na^+ and Li^+ selective but has 60% larger unitary currents in the presence of Li^+, we used Li^+ in these experiments to facilitate measurements of poorly expressing subunit combinations. The bile acid increased amiloride-sensitive Li^+ currents of heterotrimeric ENaC by 70 (7)% (n = 6 oocytes) (Figure 4), similar to the increase we observed in the presence of Na^+ (Wang et al., 2019). The bile acid also increased amiloride-sensitive currents of α_3 (70 (15)%, n = 11 oocytes) and αβ (61 (31)%, n = 7 oocytes). We observed no t-CA-dependent effect on amiloride-sensitive currents when we expressed αγ (n = 15 oocytes), nor any effect on absolute currents in uninjected oocytes (n = 8 oocytes). These data suggest that the α subunit is sufficient for ENaC sensitivity to t-CA and that co-expression of the γ subunit may dampen that response.

ENaC activation by t-CA is voltage-dependent–

We hypothesized that bile acids regulate ENaC through direct binding. Since taurine conjugated bile acids are negatively charged at physiologic pH (see Figure 1), binding at a site within the membrane-associated voltage-gradient could give rise to voltage-dependence in the dose-response curve. We therefore determined the voltage-dependence of the t-CA dose-response. Oocytes expressing ENaC were bathed in increasing doses of t-CA in TEVC experiments (Figure 5A). At the end of each dose period, voltage was varied stepwise

from −140 mV to 20 mV. Amiloride-sensitive current-voltage curves (Figure 5B) and dose-response curves (Figure 5C) suggested greater relative stimulation at −40 mV than −140 mV, consistent with greater negative potentials disfavoring binding of the negatively charged bile acid. Linear regression of the relative stimulation by t-CA showed a dependence on voltage at 100 μM and greater t-CA concentrations (Figure 5D).

The binding of a charged ligand within an electric field is governed by both the free energy of binding ($\Delta G = -RT \ln K$) and the free energy of moving the molecule across the field ($\Delta G = zF\Delta V$), where K is the dissociation constant, z is the charge of the ligand and F, V, R and T have their usual meanings. Combining both factors gives the voltage-sensitive dissociation constant K_n^V:

$$K_n^V = K_n \, exp\left(\frac{zF\delta_n V}{RT}\right) \quad (1)$$

where K_n is the intrinsic dissociation constant of the n^{th} site, and δ_n is the relative depth of the n^{th} binding site within the electric field. Fitting our data to a scheme where t-CA drives activation by binding at one site in the open-state (Figure 5F, Model A) approximated the voltage-dependent behavior we observed, but notably underestimated the voltage-dependence at high t-CA concentrations and overestimated the voltage-dependence at low t-CA concentrations (Figure 5E, dashed lines). Additional binding sites significantly improved modeling of the data. Model D had two binding sites in the open-state and one binding site in the closed-state, and well-approximated the voltage-dependence at both low and high t-CA concentrations. Simpler models are nested within Model D, which has 7 fitted parameters, and were compared to Model D by F-test. The fit to Model D was significantly better than each of the nested models: $p < 0.0001$ vs Model A with 3 fitted parameters, $p < 0.0001$ vs Model B with 5 fitted parameters, and $p = 0.002$ vs Model C with 5 fitted parameters. Adding sites to Model D did not improve the fit (not shown).

The two open-state binding sites described by K_1 and K_3 had binding affinities of 67 (4) μM and 235 (22) μM, respectively. The closed-state binding site described by K_2 had a binding affinity of 193 (25) μM. Although all binding sites were permitted to be voltage-sensitive ($\delta_n > 0$), only one of the two sites in the open-state (K_3) was voltage-sensitive, with the best fit resulting in δ_3 equal to 0.43 (0.03). This value is greater than that for amiloride, an ENaC pore blocker (Palmer, 1984; Warncke & Lindemann, 1985; Kashlan et al., 2005). The equilibrium constant between unbound states, K_o, was 0.28 (0.02) and reflected a P_o of 0.22 for unstimulated channels, in agreement with published reports (Sheng et al., 2006) and similar to the basal P_o we observed in distal renal tubules from mice on a normal diet (Figure 2C). This model suggests multiple binding sites for t-CA, with one site possibly associated with the transmembrane helices (see Figure 1B). The voltage-insensitive sites in the open and closed states could reflect either distinct or overlapping physical sites, but these data do not distinguish between these possibilities.

ENaC activation by t-HDCA is voltage-independent–

Our model for t-CA suggests that ENaC hosts a voltage-independent effector site where binding results in inhibition. Taurohyodeoxycholic acid inhibits mouse ENaC with kinetics

suggesting an allosteric mechanism rather than a pore-blocking one (Wang et al., 2019). Our t-CA model predicts that inhibition could be voltage-independent for a different bile acid if K_2 was strong relative to K_1 and K_3 (Figure 5F). To test this idea, we determined the voltage-dependent dose-response of t-HDCA on ENaC currents, as above (Figure 6). We observed similar t-HDCA dose-responses for voltages between −140 and −40 mV (Figure 6C). Indeed, linear regression of the relative inhibition by t-HDCA showed no dependence on voltage for any t-HDCA concentration (Figure 6D).

Bile acids directly bind ENaC subunits–

To test whether bile acids physically interact with ENaC, we employed a photoaffinity labeling approach (Mackinnon & Taunton, 2009). We synthesized a deoxycholic acid derivative (DCA-p; Figure 7A) bearing diazirine (purple) and terminal alkyne (orange) groups for photoaffinity labeling, as previously described (Zhuang et al., 2017). We incubated Fisher rat thyroid (FRT) cells expressing ENaC subunits, where one subunit had a C-terminal V5-epitope tag, with 50 μM DCA-p in the dark. To label probe-bound proteins, we irradiated cells with UV light, whereupon the diazirine group releases N_2 and leaves a reactive carbene intermediate that covalently bonds to adjacent macromolecules. We then processed samples to isolate labeled proteins and subjected the input, unbound, and eluted fractions to SDS-PAGE and immunoblotting using anti-V5 antibodies. With DCA-p alone, we observed apparent crosslinking for all three ENaC subunits (Figures 7B–D, competition: –).

To determine whether crosslinking was specific, we attempted to reduce crosslinking through competition. Aside from the addition of the indicated competing bile acid (1 mM) simultaneous to DCA-p addition, all other procedures were identical. We observed a reduction of crosslinking to the β subunit with competition from deoxycholic acid (DCA), and a reduction of crosslinking to the γ subunit with competition from t-CA (Figures 7C, D). We did not observe a decrease in crosslinking to the α subunit with any of the competing bile acids we tested (Figure 7B). These data demonstrate specific crosslinking to the β and γ subunits and provide evidence for multiple binding sites with varied site-specific affinities.

ENaC P_o does not affect photoaffinity labeling–

We hypothesized that bile acid binding to ENaC is state-dependent, consistent with an allosteric model of regulation. Consequently, we determined whether P_o influenced crosslinking efficiency. Mutating furin cleavage sites in both the α (R205A, R231A; α^F) and γ (R143A; γ^F) subunits decreases the channel's P_o to less than 0.1 (Sheng et al., 2006). Conversely, mutating the 'degenerin' site in the β subunit (S518K) increases the channel's P_o to 0.96 (Snyder et al., 2000; Carattino et al., 2005). As the β subunit showed the strongest specific crosslinking to DCA-p (Figure 7), we examined crosslinking to the β subunit. To account for differences in expression, we determined the relative crosslinking efficiency of the surface pool by labeling and isolating surface proteins and isolating probe-labeled proteins from the surface fraction. We measured the relative densities of the total, surface and crosslinked pools and compared them to determine the relative total expression, surface expression and crosslinking of the surface pool (Figure 8). We did not detect differences between mutants in relative total expression or the fraction of channels at the surface

(Figures 8B, C). We also found no difference between mutants in the fraction of the surface pool that was crosslinked to DCA-p (Figure 8D), suggesting that P_o did not affect DCA-p crosslinking efficiency of the surface pool. These data indicate that DCA-p crosslinking is not state-dependent, suggesting the presence of binding sites in both states (see Figure 5F) and/or that both the open and closed states were sampled during the experiment.

Amiloride does not compete for bile acid binding–

Amiloride inhibits ENaC by binding within the transmembrane helical bundle (see Figure 1B) and interfering with ion permeation (Schild et al., 1997; Kashlan et al., 2005; Sheng et al., 2005). Data in Figure 5 and previous work showing that the degenerin site in the transmembrane helices influences the effect of bile acids (Ilyaskin et al., 2016) raise the possibility that the amiloride and bile acid binding sites overlap. To investigate whether amiloride competes with bile acid binding, we performed crosslinking experiments as described above in the presence or absence of 100 μM amiloride. Comparisons of the quantified densities showed that amiloride had no effect on photoaffinity labeling by DCA-p (Figure 9).

Discussion

Several lines of evidence strongly support bile acid regulation of ENaC through an allosteric mechanism, where bile acids directly bind the channel and modulate its P_o. We previously showed that effects on ENaC currents depend on bile acid functional groups, suggesting a specific interaction (Wang et al., 2019). The kinetics of regulation were similar for all bile acids, on the order of seconds, and like other allosteric ENaC regulators. This accords with re-equilibration between functional states being rate-limiting rather than bile acid effects on membrane properties. Here, we show that t-CA regulation of ENaC is voltage-sensitive. We found that the data were best explained using a model having a single voltage-sensitive open-state binding site and both open-state and closed-state voltage-insensitive binding sites. The notion of multiple binding sites is supported by our results showing that α_3 channels were bile acid sensitive, and that the β and γ subunits were specifically crosslinked in photoaffinity labeling experiments. Consistent with our regulation model, here we show for the first time that bile acids regulate ENaC in native tissues.

Bile acids likely regulate ENaC function in animals. The identity, concentration, and localization of bile acids vary. Hepatocytes synthesize primary bile acids (e.g., t-CA), which then travel through the biliary tree into the gut. Modification by gut microbiota produces secondary bile acids (e.g., DCA, t-HDCA). Most bile acids are recycled to the liver through the portal vein. Reflecting recycling, healthy subject bile acid pools include both primary and secondary bile acids (Brandl et al., 2018), and both may be relevant in regulating ENaC in the biliary tree and gut. Here, ENaC has a role in regulating luminal fluids (Zeissig et al., 2008; Li et al., 2016). As bile acids variously regulate ENaC function, these compounds may account for part of the microbiome's influence on intestinal ion transport (Barrett, 2017). Relatively small quantities of bile acids escape the enterohepatic circulation and have important signaling roles (Chiang, 2013), but are unlikely to regulate ENaC outside of the gut and liver given the ~0.1 mM binding affinity we report here.

Advanced liver disease may disrupt bile flow (i.e., cholestasis), leading to conjugated primary bile acids predominating and greatly elevating blood and urine bile acid levels as urine becomes the primary excretion vehicle (Miura et al., 2011; Brandl et al., 2018). Given the correlation between blood and urine bile acid levels and the significant reduction in urine volumes observed in cirrhotic patients (Miura et al., 2011; Wong, 2013), urine bile acid levels likely fall into the 0.1 – 1 mM range for the sickest patients. Whether high urinary concentrations correspond to high concentrations in the CCD is uncertain. If so, bile acids may aberrantly regulate ENaC in the kidney. Notably, liver disease patients often exhibit Na^+ and fluid retention, and electrolyte imbalances (Eisenmenger et al., 1950). Elevated aldosterone levels activate renal ENaC through the mineralocorticoid receptor and have long been recognized as contributing to liver disease-associated fluid retention (Kerr et al., 1958). Accordingly, mineralocorticoid receptor antagonists are important tools in treating liver disease associated ascites and edema. However, aldosterone is not elevated in all patients exhibiting fluid retention (Wilkinson & Williams, 1980). Our data showing t-CA activation of ENaC in distal renal tubular cells suggest that there may be an aldosterone-independent mechanism that activates ENaC in liver disease. Indeed, ENaC blockade has been proposed as an alternative to targeting the mineralocorticoid receptor for patients without increased aldosterone (Angeli et al., 1994). This hypothesis will need further investigation.

The dependence of ENaC regulation on specific bile acid functional groups suggests competing mechanistic models. In one model, bile acids bind one or more binding sites, and the identity of the occupied site(s) determines the effect on ENaC activity (see Figure 5F). In this model, bile acids have varied effects because of their relative affinities for each of the sites. In a second model, occupied sites are similar, but the regulatory effect varies dependent on bile functional groups. In this model, similar binding sites may be occupied, but bile acid functional groups at each site stabilize specific conformations. Our data favor the first model. DCA reduced photoaffinity labeling of the β subunit while t-CA reduced photoaffinity labeling of the γ subunit. These data suggest that sites involving the β or γ subunits preferentially bind DCA or t-CA, respectively. Activation by t-CA was voltage-sensitive while inhibition by t-HDCA was not. These data suggest that t-HDCA has poor affinity for any voltage-sensitive site(s).

Our finding that t-CA activation is voltage-sensitive fits with previous work providing evidence for a site associated with the pore (Ilyaskin et al., 2016). Ilyaskin and coworkers found that mutations near the β subunit degenerin site three helical turns extracellular to a conserved Gly/Ser-X-Ser motif implicated in ion selectivity reduced activation of human ENaC by chenodeoxycholic acid. Amiloride blocks ENaC by binding at a site between the Ilyaskin site and the Gly/Ser-X-Ser motif (Schild et al., 1997; Sheng et al., 2005). Our data suggest an electric depth for t-CA binding ($\delta = 0.4$) greater than that for amiloride binding ($\delta = 0.15–0.2$, (Palmer, 1985; Kashlan et al., 2005)). Our data also provide no evidence for competition between amiloride and bile acid binding. A binding site that avoids blocking channel currents near the Ilyaskin site could be consistent with the lack of competition and differences in both δ values and effects on ENaC function.

Our data also shed light on the properties of noncanonical channels. ENaC subunit expression varies and is noncoordinately regulated, leading to situations where one or

more subunits may be limiting (Weisz & Johnson, 2003). In these circumstances, ENaC subunits form trimers (Stewart et al., 2011) with some subunit combinations yielding distinct functional properties. For example, αβ was reported to be constitutively open ($P_o \approx 1$) in the presence of Li^+ based on single channel data (Fyfe & Canessa, 1998). However, we found that t-CA increased αβ–mediated Li^+ currents by 60% (Figure 4). These data place an upper limit of 0.63 on the average P_o of αβ in the presence of Li^+. Challenges in patch clamp experiments arising from low expression or long open times may contribute to the discrepancy. Our data also place an upper limit of 0.59 for the average P_o of α_3, consistent with a blend of high P_o (0.85) and low P_o (0.13) α_3 populations (Kelly et al., 2003). In contrast, the lack of an effect of t-CA on αγ precludes further interpretation. As a reversible ENaC activator, t-CA may be useful as an experimental tool to probe ENaC function, and may have advantages over using proteases, which are irreversible ENaC activators. For example, t-CA did not activate ENaC in distal colon from animals on a low salt diet, hinting that channels may have already undergone activating cleavage under these conditions. Evidence shows that dietary maneuvers that increase aldosterone levels promote activating cleavage of ENaC subunits in the aldosterone-sensitive distal nephron (Carattino et al., 2014; Frindt et al., 2021), though this has not yet been demonstrated in the distal colon.

In conclusion, bile acids regulate ENaC expressed in the renal distal tubule and colon, supporting the notion that this regulation may contribute to physiological or pathophysiological processes. Bile acids directly bind ENaC and show specific binding affinities to each of several sites. We propose that bile acids bind to sites in both the extracellular and transmembrane domains of NaC and modulate channel activity.

Supplementary Material

Refer to Web version on PubMed Central for supplementary material.

Acknowledgements

The authors thank Dr. Shujie Shi for helpful discussions.

Funding

This work was supported by grants from NIDDK, National Institutes of Health, DK125439 (OBK), DK095029 (OP), DK117865 (OP), a grant from The Pittsburgh Liver Research Center (OBK) and a grant from the American Heart association (EIA35260097 to OP). The Pittsburgh Liver Research Center was supported by P30 DK120531 from NIDDK. The Pittsburgh Center for Kidney Research was supported by P30 DK079307 from NIDDK.

First author profile:

Xue-Ping Wang received her PhD degree in Biochemistry and Structural Biology from the University of Science and Technology of China in Hefei. She then received her postdoctoral

training in the Department of Medicine, University of Pittsburgh. She is currently an Instructor at the University of Pittsburgh School of Medicine. Her current research projects investigate mechanisms of ion channel functional regulation and their role in physiology.

Data Availability

All data analyzed are included in the figures.

Abbreviations used:

ENaC	epithelial Na^+ channel
P_o	open probability
t-CA	taurocholic acid
t-HDCA	taurohyodeoxycholic acid
I_{SC}	short-circuit currents
FRT	Fisher rat thyroid
DCA	deoxycholic acid
t-DCA	taurodeoxycholic acid

References

Ahn YJ, Brooker DR, Kosari F, Harte BJ, Li J, Mackler SA & Kleyman TR. (1999). Cloning and functional expression of the mouse epithelial sodium channel. Am J Physiol 277, F121–129. [PubMed: 10409305]

Angeli P, Dalla Pria M, De Bei E, Albino G, Caregaro L, Merkel C, Ceolotto G & Gatta A. (1994). Randomized clinical study of the efficacy of amiloride and potassium canrenoate in nonazotemic cirrhotic patients with ascites. Hepatology 19, 72–79. [PubMed: 8276370]

Barrett KE. (2017). Endogenous and exogenous control of gastrointestinal epithelial function: building on the legacy of Bayliss and Starling. The Journal of physiology 595, 423–432. [PubMed: 27284010]

Bertog M, Cuffe JE, Pradervand S, Hummler E, Hartner A, Porst M, Hilgers KF, Rossier BC & Korbmacher C. (2008). Aldosterone responsiveness of the epithelial sodium channel (ENaC) in colon is increased in a mouse model for Liddle's syndrome. The Journal of physiology 586, 459–475. [PubMed: 18006588]

Brandl K, Hartmann P, Jih LJ, Pizzo DP, Argemi J, Ventura-Cots M, Coulter S, Liddle C, Ling L, Rossi SJ, DePaoli AM, Loomba R, Mehal WZ, Fouts DE, Lucey MR, Bosques-Padilla F, Mathurin P, Louvet A, Garcia-Tsao G, Verna EC, Abraldes JG, Brown RS Jr., Vargas V, Altamirano J, Caballeria J, Shawcross D, Starkel P, Ho SB, Bataller R & Schnabl B. (2018). Dysregulation of serum bile acids and FGF19 in alcoholic hepatitis. J Hepatol 69, 396–405. [PubMed: 29654817]

Bruns JB, Carattino MD, Sheng S, Maarouf AB, Weisz OA, Pilewski JM, Hughey RP & Kleyman TR. (2007). Epithelial Na^+ channels are fully activated by furin- and prostasin-dependent release of an inhibitory peptide from the g-subunit. J Biol Chem 282, 6153–6160. [PubMed: 17199078]

Canessa CM, Schild L, Buell G, Thorens B, Gautschi I, Horisberger JD & Rossier BC. (1994). Amiloride-sensitive epithelial Na^+ channel is made of three homologous subunits. Nature 367, 463–467. [PubMed: 8107805]

Carattino MD, Edinger RS, Grieser HJ, Wise R, Neumann D, Schlattner U, Johnson JP, Kleyman TR & Hallows KR. (2005). Epithelial sodium channel inhibition by AMP-activated protein kinase in oocytes and polarized renal epithelial cells. J Biol Chem 280, 17608–17616. [PubMed: 15753079]

Carattino MD, Mueller GM, Palmer LG, Frindt G, Rued AC, Hughey RP & Kleyman TR. (2014). Prostasin interacts with the epithelial Na+ channel and facilitates cleavage of the gamma-subunit by a second protease. Am J Physiol Renal Physiol 307, F1080–1087. [PubMed: 25209858]

Carattino MD, Passero CJ, Steren CA, Maarouf AB, Pilewski JM, Myerburg MM, Hughey RP & Kleyman TR. (2008). Defining an inhibitory domain in the a-subunit of the epithelial sodium channel. Am J Physiol Renal Physiol 294, F47–52. [PubMed: 18032549]

Chiang JY. (2013). Bile acid metabolism and signaling. Compr Physiol 3, 1191–1212. [PubMed: 23897684]

Eisenmenger WJ, Blondheim SH, Bongiovanni AM & Kunkel HG. (1950). Electrolyte studies on patients with cirrhosis of the liver. J Clin Invest 29, 1491–1499. [PubMed: 14794777]

Frindt G & Palmer LG. (2015). Acute effects of aldosterone on the epithelial Na channel in rat kidney. Am J Physiol Renal Physiol 308, F572–578. [PubMed: 25520012]

Frindt G, Shi S, Kleyman TR & Palmer LG. (2021). Cleavage state of gammaENaC in mouse and rat kidneys. Am J Physiol Renal Physiol 320, F485–F491. [PubMed: 33522411]

Fyfe GK & Canessa CM. (1998). Subunit composition determines the single channel kinetics of the epithelial sodium channel. The Journal of general physiology 112, 423–432. [PubMed: 9758861]

Garty H & Palmer LG. (1997). Epithelial sodium channels: function, structure, and regulation. Physiol Rev 77, 359–396. [PubMed: 9114818]

Grundy D (2015). Principles and standards for reporting animal experiments in The Journal of Physiology and Experimental Physiology. The Journal of physiology 593, 2547–2549. [PubMed: 26095019]

Heidrich E, Carattino MD, Hughey RP, Pilewski JM, Kleyman TR & Myerburg MM. (2015). Intracellular Na+ regulates epithelial Na+ channel maturation. J Biol Chem 290, 11569–11577. [PubMed: 25767115]

Hughey RP, Mueller GM, Bruns JB, Kinlough CL, Poland PA, Harkleroad KL, Carattino MD & Kleyman TR. (2003). Maturation of the epithelial Na^+ channel involves proteolytic processing of the α- and ɣ-subunits. J Biol Chem 278, 37073–37082. [PubMed: 12871941]

Ilyaskin AV, Diakov A, Korbmacher C & Haerteis S. (2016). Activation of the Human Epithelial Sodium Channel (ENaC) by Bile Acids Involves the Degenerin Site. J Biol Chem 291, 19835–19847. [PubMed: 27489102]

Kashlan OB, Sheng S & Kleyman TR. (2005). On the interaction between amiloride and its putative a-subunit epithelial Na^+ channel binding site. J Biol Chem 280, 26206–26215. [PubMed: 15908426]

Keely SJ, Urso A, Ilyaskin AV, Korbmacher C, Bunnett NW, Poole DP & Carbone SE. (2022). Contributions of bile acids to gastrointestinal physiology as receptor agonists and modifiers of ion channels. Am J Physiol Gastrointest Liver Physiol 322, G201–G222. [PubMed: 34755536]

Kelly O, Lin C, Ramkumar M, Saxena NC, Kleyman TR & Eaton DC. (2003). Characterization of an amiloride binding region in the a-subunit of ENaC. Am J Physiol Renal Physiol 285, F1279–1290. [PubMed: 12928313]

Kerr DN, Read AE, Haslam RM & Sherlock S. (1958). The use of a steroidal spirolactone in the treatment of ascites in hepatic cirrhosis. Lancet 2, 1084–1087. [PubMed: 13599489]

Li Q, Kresge C, Bugde A, Lamphere M, Park JY & Feranchak AP. (2016). Regulation of mechanosensitive biliary epithelial transport by the epithelial Na(+) channel. Hepatology 63, 538–549. [PubMed: 26475057]

Mackinnon AL & Taunton J. (2009). Target Identification by Diazirine Photo-Cross-linking and Click Chemistry. Curr Protoc Chem Biol 1, 55–73. [PubMed: 23667793]

Mamenko M, Zaika O, Doris PA & Pochynyuk O. (2012a). Salt-dependent inhibition of epithelial Na+ channel-mediated sodium reabsorption in the aldosterone-sensitive distal nephron by bradykinin. Hypertension 60, 1234–1241. [PubMed: 23033373]

Mamenko M, Zaika O, Ilatovskaya DV, Staruschenko A & Pochynyuk O. (2012b). Angiotensin II increases activity of the epithelial Na+ channel (ENaC) in distal nephron additively to aldosterone. J Biol Chem 287, 660–671. [PubMed: 22086923]

Mamenko M, Zaika O, Prieto MC, Jensen VB, Doris PA, Navar LG & Pochynyuk O. (2013). Chronic angiotensin II infusion drives extensive aldosterone-independent epithelial Na+ channel activation. Hypertension 62, 1111–1122. [PubMed: 24060890]

Mamenko M, Zaika O, Tomilin V, Jensen VB & Pochynyuk O. (2018). Compromised regulation of the collecting duct ENaC activity in mice lacking AT1a receptor. J Cell Physiol 233, 7217–7225. [PubMed: 29574718]

Mironova E, Bugay V, Pochynyuk O, Staruschenko A & Stockand JD. (2013). Recording ion channels in isolated, split-opened tubules. Methods Mol Biol 998, 341–353. [PubMed: 23529443]

Miura R, Tanaka A & Takikawa H. (2011). Urinary bile acid sulfate levels in patients with primary biliary cirrhosis. Hepatol Res 41, 358–363. [PubMed: 21348908]

Nickerson AJ, Rottgen TS & Rajendran VM. (2021). Activation of KCNQ (KV7) K(+) channels in enteric neurons inhibits epithelial Cl(−) secretion in mouse distal colon. Am J Physiol Cell Physiol 320, C1074–C1087. [PubMed: 33852365]

Noreng S, Bharadwaj A, Posert R, Yoshioka C & Baconguis I. (2018). Structure of the human epithelial sodium channel by cryo-electron microscopy. Elife 7.

Palmer LG. (1984). Voltage-dependent block by amiloride and other monovalent cations of apical Na channels in the toad urinary bladder. J Membr Biol 80, 153–165. [PubMed: 6090670]

Palmer LG. (1985). Interactions of amiloride and other blocking cations with the apical Na channel in the toad urinary bladder. J Membr Biol 87, 191–199. [PubMed: 2416933]

Pearce D, Soundararajan R, Trimpert C, Kashlan OB, Deen PM & Kohan DE. (2015). Collecting duct principal cell transport processes and their regulation. Clinical journal of the American Society of Nephrology : CJASN 10, 135–146. [PubMed: 24875192]

Prieto MC, Reverte V, Mamenko M, Kuczeriszka M, Veiras LC, Rosales CB, McLellan M, Gentile O, Jensen VB, Ichihara A, McDonough AA, Pochynyuk OM & Gonzalez AA. (2017). Collecting duct prorenin receptor knockout reduces renal function, increases sodium excretion, and mitigates renal responses in ANG II-induced hypertensive mice. Am J Physiol Renal Physiol 313, F1243–F1253. [PubMed: 28814438]

Rotin D & Staub O. (2021). Function and Regulation of the Epithelial Na(+) Channel ENaC. Compr Physiol 11, 2017–2045. [PubMed: 34061979]

Schild L, Schneeberger E, Gautschi I & Firsov D. (1997). Identification of amino acid residues in the a, b, and g subunits of the epithelial sodium channel (ENaC) involved in amiloride block and ion permeation. The Journal of general physiology 109, 15–26. [PubMed: 8997662]

Schmidt A, Alsop RJ, Rimal R, Lenzig P, Joussen S, Gervasi NN, Khondker A, Grunder S, Rheinstadter MC & Wiemuth D. (2018). Modulation of DEG/ENaCs by Amphiphiles Suggests Sensitivity to Membrane Alterations. Biophysical journal 114, 1321–1335. [PubMed: 29590590]

Sheng S, Carattino MD, Bruns JB, Hughey RP & Kleyman TR. (2006). Furin cleavage activates the epithelial Na^+ channel by relieving Na^+ self-inhibition. Am J Physiol Renal Physiol 290, F1488–1496. [PubMed: 16449353]

Sheng S, Perry CJ, Kashlan OB & Kleyman TR. (2005). Side chain orientation of residues lining the selectivity filter of epithelial Na^+ channels. J Biol Chem 280, 8513–8522. [PubMed: 15611061]

Snyder PM, Bucher DB & Olson DR. (2000). Gating induces a conformational change in the outer vestibule of ENaC. The Journal of general physiology 116, 781–790. [PubMed: 11099347]

Stewart AP, Haerteis S, Diakov A, Korbmacher C & Edwardson JM. (2011). Atomic force microscopy reveals the architecture of the epithelial sodium channel (ENaC). J Biol Chem 286, 31944–31952. [PubMed: 21775436]

Terker AS, Yarbrough B, Ferdaus MZ, Lazelle RA, Erspamer KJ, Meermeier NP, Park HJ, McCormick JA, Yang CL & Ellison DH. (2016). Direct and Indirect Mineralocorticoid Effects Determine Distal Salt Transport. Journal of the American Society of Nephrology : JASN 27, 2436–2445. [PubMed: 26712527]

Wang XP, Im SJ, Balchak DM, Montalbetti N, Carattino MD, Ray EC & Kashlan OB. (2019). Murine epithelial sodium (Na(+)) channel regulation by biliary factors. J Biol Chem 294, 10182–10193. [PubMed: 31092599]

Warncke J & Lindemann B. (1985). Voltage dependence of Na channel blockage by amiloride: relaxation effects in admittance spectra. J Membr Biol 86, 255–265. [PubMed: 2413213]

Weisz OA & Johnson JP. (2003). Noncoordinate regulation of ENaC: paradigm lost? Am J Physiol Renal Physiol 285, F833–842. [PubMed: 14532162]

Wiemuth D, Lefevre CM, Heidtmann H & Grunder S. (2014). Bile acids increase the activity of the epithelial Na+ channel. Pflugers Arch 466, 1725–1733. [PubMed: 24292109]

Wilkinson SP & Williams R. (1980). Renin-angiotensin-aldosterone system in cirrhosis. Gut 21, 545–554. [PubMed: 7000629]

Wong F (2013). Acute renal dysfunction in liver cirrhosis. Gastroenterol Hepatol (N Y) 9, 830–832. [PubMed: 24772051]

Zeissig S, Bergann T, Fromm A, Bojarski C, Heller F, Guenther U, Zeitz M, Fromm M & Schulzke JD. (2008). Altered ENaC expression leads to impaired sodium absorption in the noninflamed intestine in Crohn's disease. Gastroenterology 134, 1436–1447. [PubMed: 18355814]

Zhuang S, Li Q, Cai L, Wang C & Lei X. (2017). Chemoproteomic Profiling of Bile Acid Interacting Proteins. ACS Cent Sci 3, 501–509. [PubMed: 28573213]

Key Points

- Recent studies have shown that bile acids regulate ENaC in vitro. Here we investigated whether bile acids regulate ENaC in native tissues and whether bile acids directly bind the channel.
- We found that bile acids regulate ENaC expressed in the mouse cortical collecting duct and mouse colon by modulating open probability.
- Photoaffinity labeling experiments showed specific binding to the β and γ subunits of the channel, while channels comprising only α subunits were sensitive to taurocholic acid in functional experiments using *Xenopus* oocytes.
- Taurocholic acid regulation of ENaC was voltage-dependent, providing evidence for binding to pore-forming helices.
- Our data indicate that bile acids are ENaC regulatory effectors that may have a role in the physiology and pathophysiology of several systems.

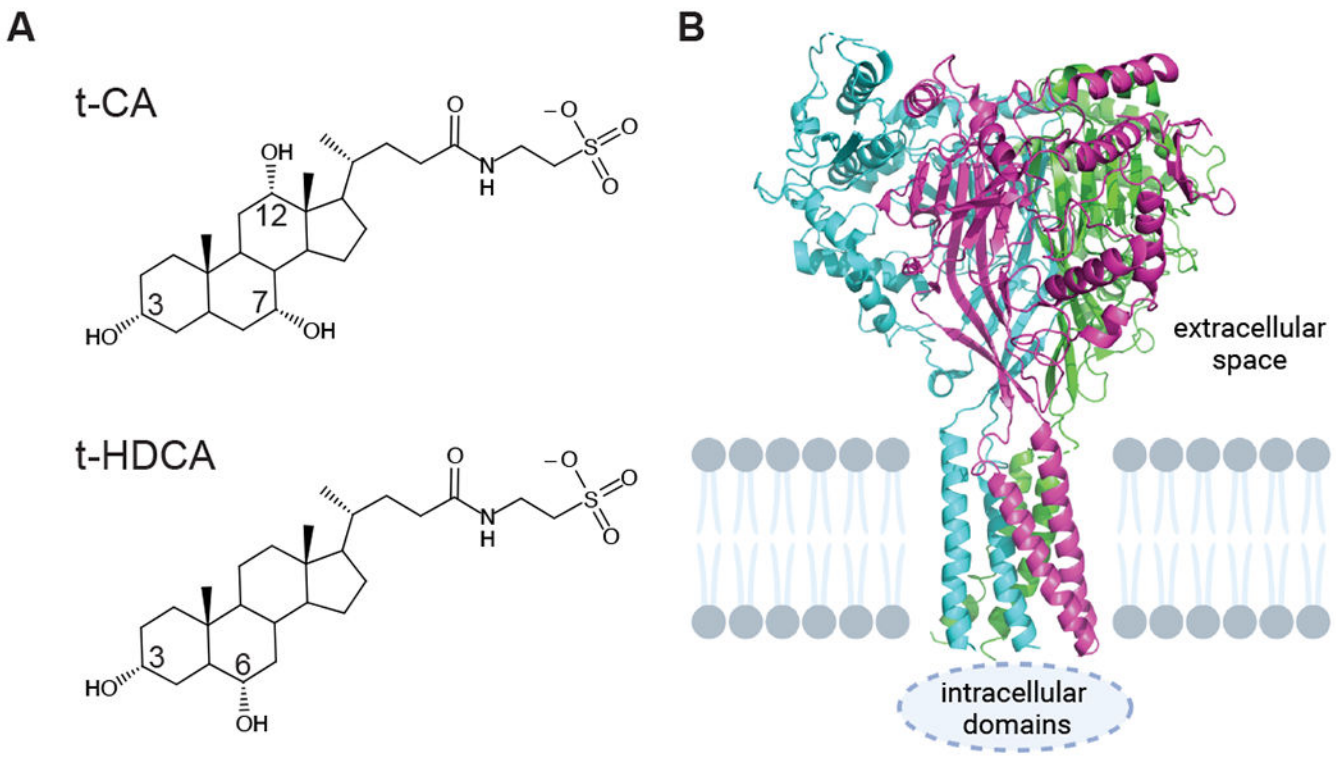

Figure 1. Bile acid and ENaC structures.

A, Structures of t-CA and t-HDCA, with positions of key functional groups numbered. Downward bonds face the hydrophilic side (α side) and upward bonds face the hydrophobic side (β side). Taurine conjugation adds a sulfonate group ($pK_a < 2$), which remains ionized at physiologic pH. **B**, Cartoon of ENaC structure (pdb code 6BQN (Noreng et al., 2018)) colored by subunit with approximate location of membrane indicated. Created with BioRender.com

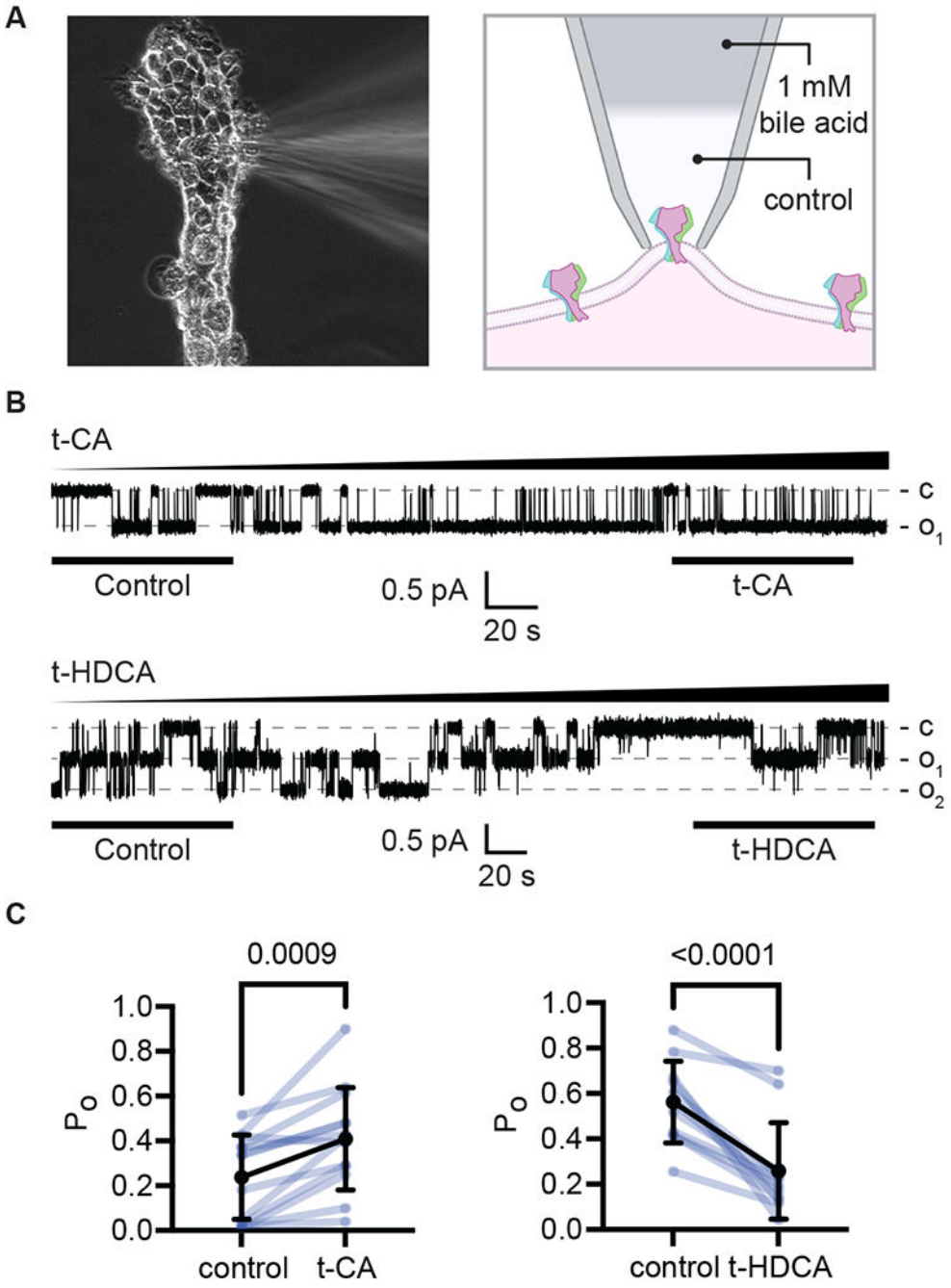

Figure 2. Bile acids regulate ENaC P_o in split open mouse distal renal tubules.

A, Distal renal tubules were isolated from mice and subjected to cell-attached patch using pipettes backfilled with either 1 mM t-CA or 1 mM t-HDCA. **B**, Representative continuous current traces with $-V_p = -60$ mV, during which bile acids diffused towards the tip of the pipette. Inward currents are downward, and the number of open channels is indicated by dashed lines. P_o was estimated from the indicated time spans representing the control and diffused conditions. **C**, Effect of bile acids on ENaC P_o. P_o determined from control and diffused conditions were compared using paired Student's t-test. Individual experiments

(blue; $n = 13$ collecting ducts for t-CA; $n = 11$ collecting ducts for t-HDCA) and summary statistics (mean (SD)) are shown. Created with BioRender.com

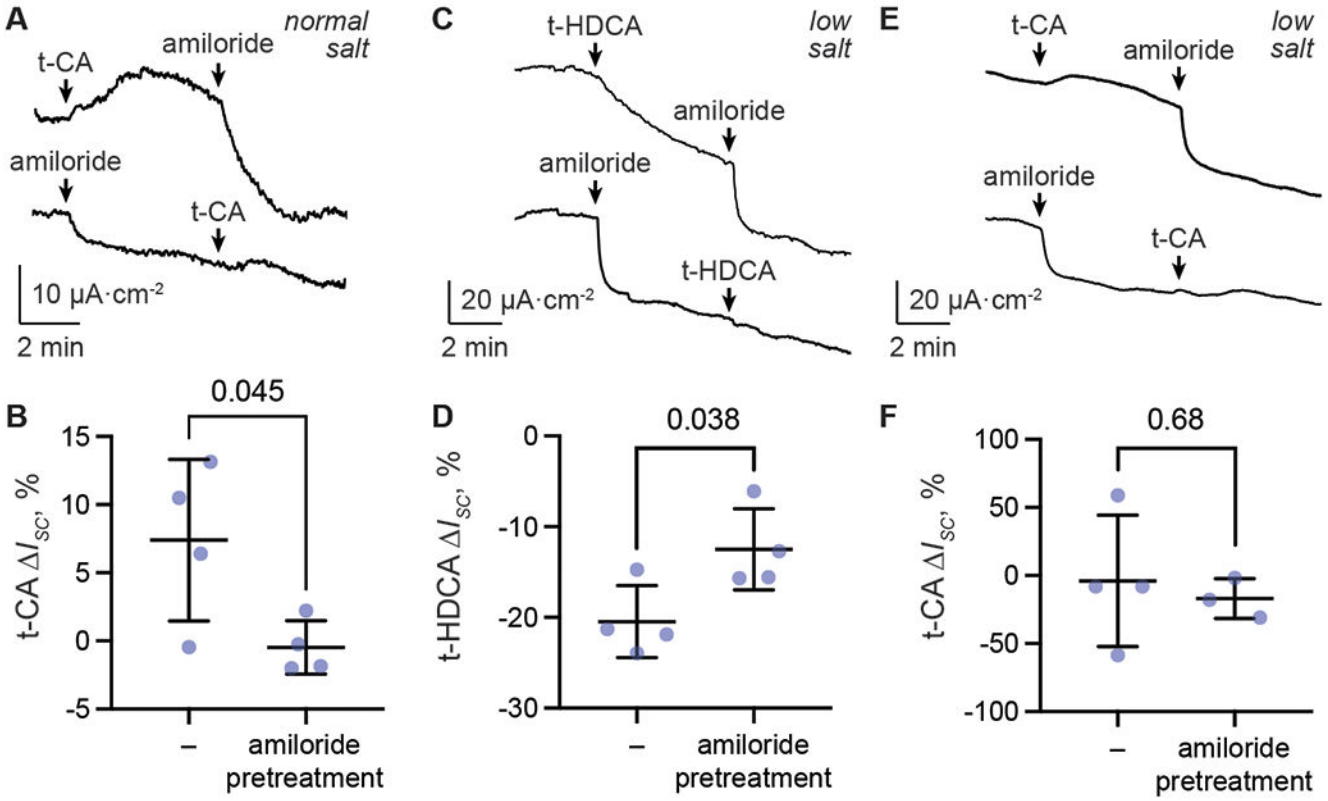

Figure 3. Bile acids regulate ENaC currents in the distal colon.

Colons isolated from mice on a normal salt diet (**A**), or after 9-10 days on a low Na^+ diet (**C, E**) were mounted in an Ussing chamber for I_{SC} measurements. After tissue equilibration, baseline currents were measured for at least 5 minutes before the addition of the first compound. Basal I_{SC} averaged 76 (15) μA/cm^2 for colons from mice on a normal salt diet, and 117 (43) μA/cm^2 for colons from mice on a low salt diet. 1 mM t-CA, 1 mM t-HDCA, or 100 μM amiloride were added to the apical bath as indicated. **B, D, F**, The effect of each compound on I_{SC} (ΔI_{SC}) was determined by measurements taken 4 min apart: 30 s before and 3.5 min after compound addition. The value of ΔI_{SC} was then normalized to the baseline current in the same recording to account for inter-animal variability in starting I_{SC}. t-CA- and t-HDCA-induced ΔI_{SC} in the absence or presence of amiloride were compared by Student's t test. Individual experiments (blue; $n = 3$ colons from mice fed a low salt diet for t-CA with amiloride pretreatment; $n = 4$ colons for other groups) and summary statistics (mean (SD)) are shown.

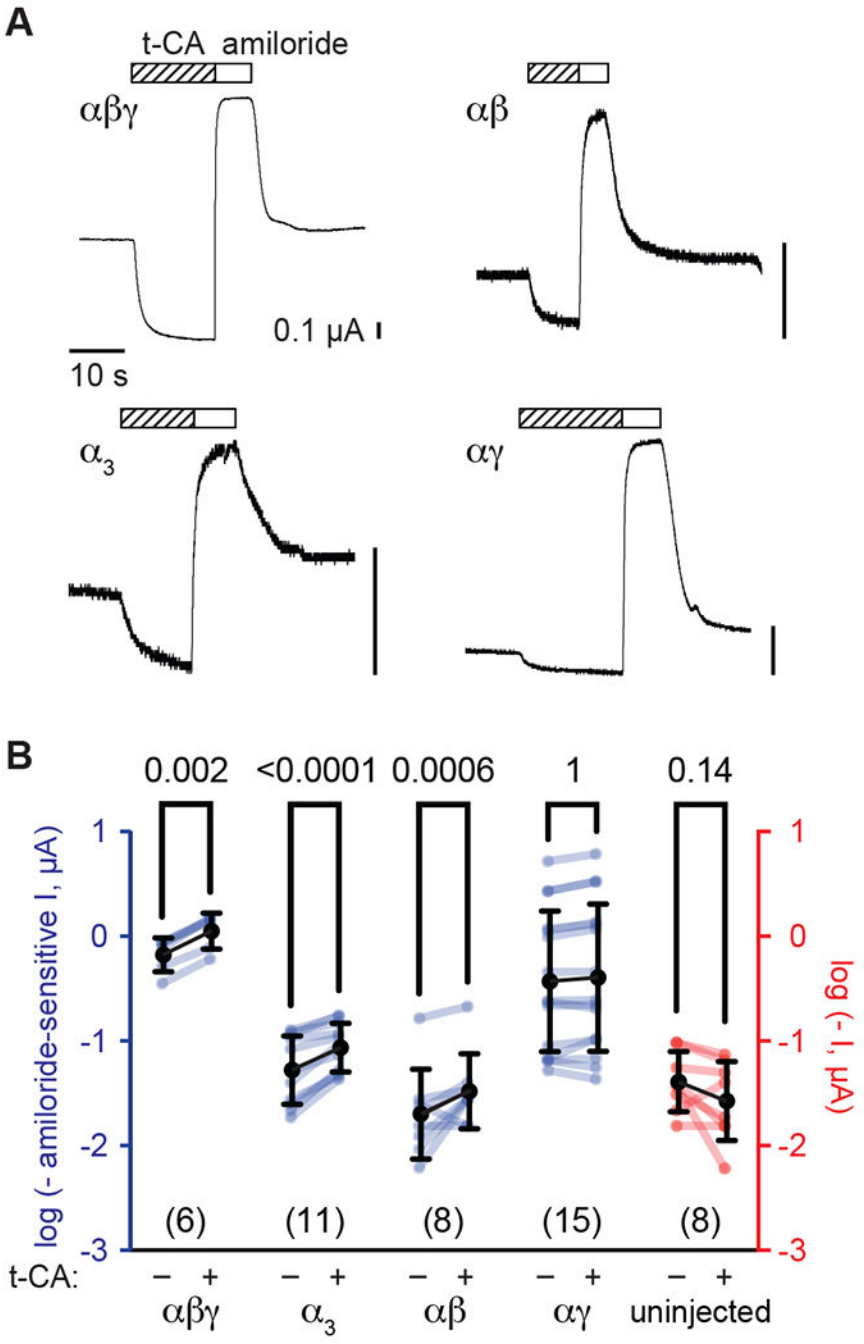

Figure 4. Effect of subunit composition on ENaC response to t-CA.

A, Currents from *Xenopus* oocytes expressing ENaC subunits shown were assessed by two-electrode voltage clamp at −100 mV. Recordings were performed in a buffer containing 110 mM Li^+, and supplemented with 1 mM t-CA or 100 μM amiloride, as indicated. Currents at baseline and in the presence of t-CA or amiloride were measured at the end of each treatment period. **B**, Amiloride-sensitive currents (blue) in the absence (−) or presence (+) of t-CA were transformed as *log(−current)* and plotted. Absolute currents (red) were similarly plotted for uninjected oocytes. Summary statistics are mean (SD). Transformed

amiloride-sensitive currents were analyzed by repeated measures two-way ANOVA, with Sidak's multiple comparison test to examine the effect of t-CA. Transformed absolute currents from uninjected oocytes were analyzed by paired Student's t test. The number of oocytes measured for each group is shown in parentheses.

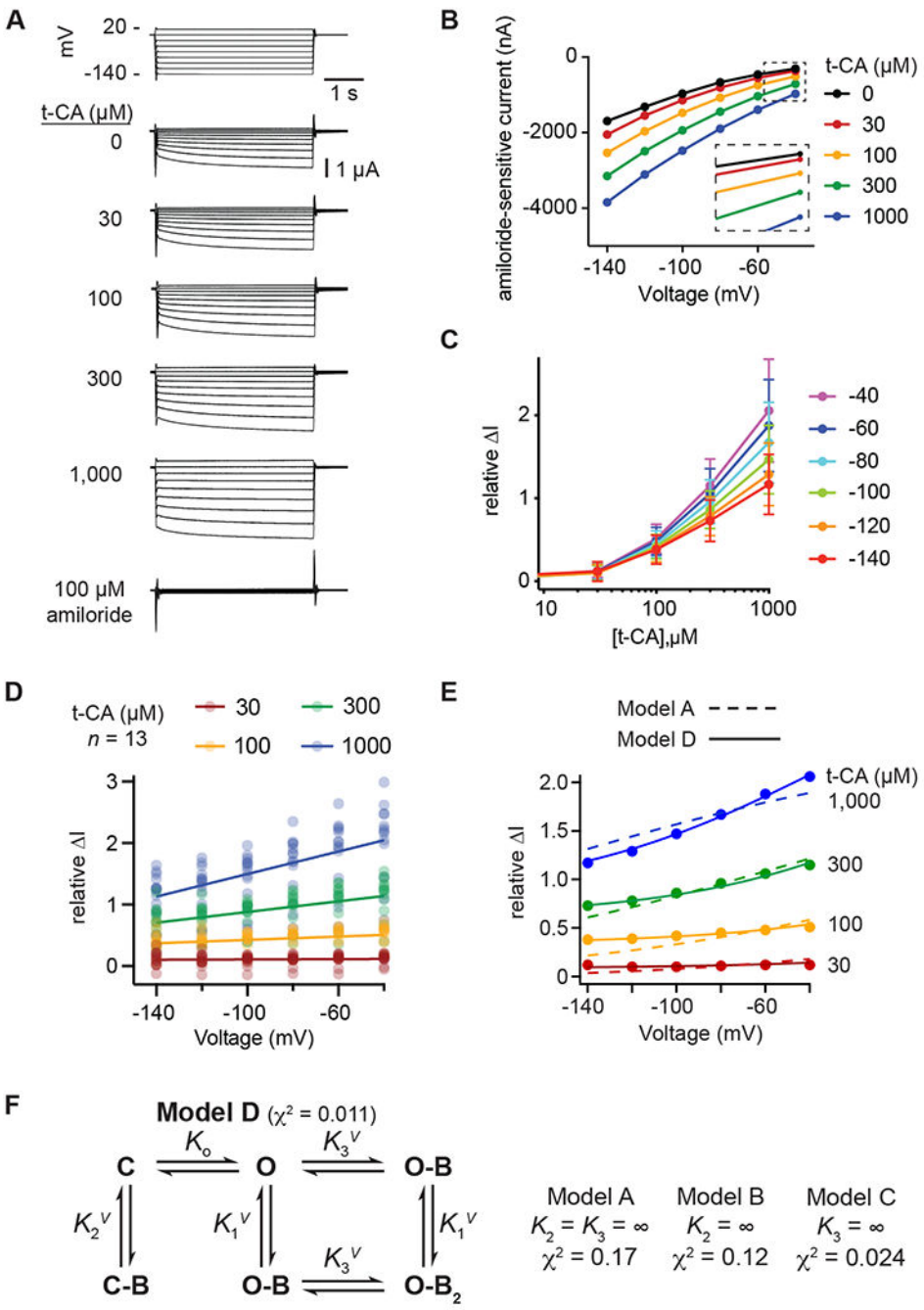

Figure 5. ENaC regulation by t-CA is voltage-dependent.

A, Oocytes expressing α, β, and γ ENaC subunits were bathed in a 110 mM Na^+ solution supplemented with t-CA or amiloride as indicated. After 60 s for each t-CA dose, or 20 s for amiloride, currents were recorded while varying voltage in 20 mV steps for 4 s, as shown in the representative experiment. Steady-state currents at each voltage (recorded at 3.8 s) were subsequently analyzed. **B**, The amiloride-sensitive I–V curve from the representative experiment is plotted for each t-CA dose, with an inset highlighting greater relative stimulation at less negative potentials. **C**, The relative t-CA dose-response for

each voltage is plotted and was determined as $\Delta I = I_X/I_0 - 1$, where I_0 and I_X are the amiloride-sensitive currents at baseline and a given t-CA dose, respectively. Data shown are mean (SD), $n = 13$ oocytes. Individual points are shown in panel D. **D-E**, The t-CA dose-response data were replotted as a function of voltage, with individual data points in D and mean values in E. Linear regression was performed for each t-CA dose (D), and gave R^2 values of 0.19 for 30 μM t-CA ($p = 0.38$), 0.98 for 100 μM t-CA ($p = 0.0002$), and 0.99 for both 300 and 1000 μM t-CA ($p < 0.0001$). **F**, Relative ΔI vs voltage data were fit to various models of regulation. The simplest model considered (Model A, dashed lines in panel **E**) had 3 states, a closed-state (C), an open-state (O), and an open-state with the bile acid bound at one site (O-B). Equilibrium constants between these states are K_o = [O]/[C] and K_1 = [O][B]/[O-B], and K_1 was permitted to have voltage-dependence according to $K_1^V = K_1 \cdot e^{zF\delta V/RT}$. Additional binding sites were defined analogously. Models A, B, and C are nested within Model D by setting the indicated binding constant(s) to ∞. The fit to the best model (Model D, solid lines in panel E) is shown.

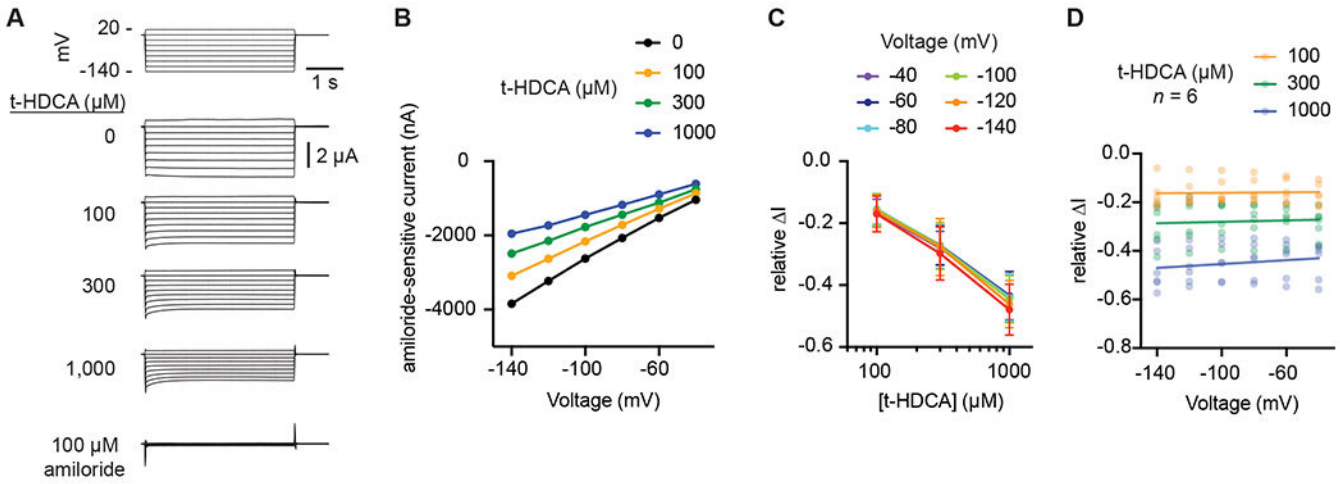

Figure 6. ENaC regulation by t-HDCA is voltage-independent.

A, Oocytes expressing α, β, and γ ENaC subunits were bathed in a 110 mM Na^+ solution supplemented with t-HDCA or amiloride as indicated. After 60 s for each t-HDCA dose, or 20 s for amiloride, currents were recorded while varying voltage in 20 mV steps for 4 s, as shown in the representative experiment. Steady-state currents at each voltage (recorded at 3.8 s) were subsequently analyzed. **B**, The amiloride-sensitive I–V curve from the representative experiment is plotted for each t-HDCA dose. **C**, The relative t-HDCA dose-response at each voltage is plotted and was determined as $\Delta I = I_X/I_0 - 1$, where I_0 and I_X are the amiloride-sensitive currents at baseline and a given t-HDCA dose, respectively. Data shown are mean (SD), $n = 6$ oocytes. **D**, The t-HDCA dose-response data were replotted as a function of voltage, with individual measurements shown as colored circles. Data at each voltage were fit by linear regression, with values of $R^2 = 0.001$, 0.005, and 0.03 for 100, 300, and 1000 μM t-HDCA, respectively. None of the slopes were significantly non-zero: $p = 0.83$ for 100 μM t-HDCA, $p = 0.68$ for 300 μM t-HDCA, and $p = 0.28$ for 1000 μM t-HDCA.

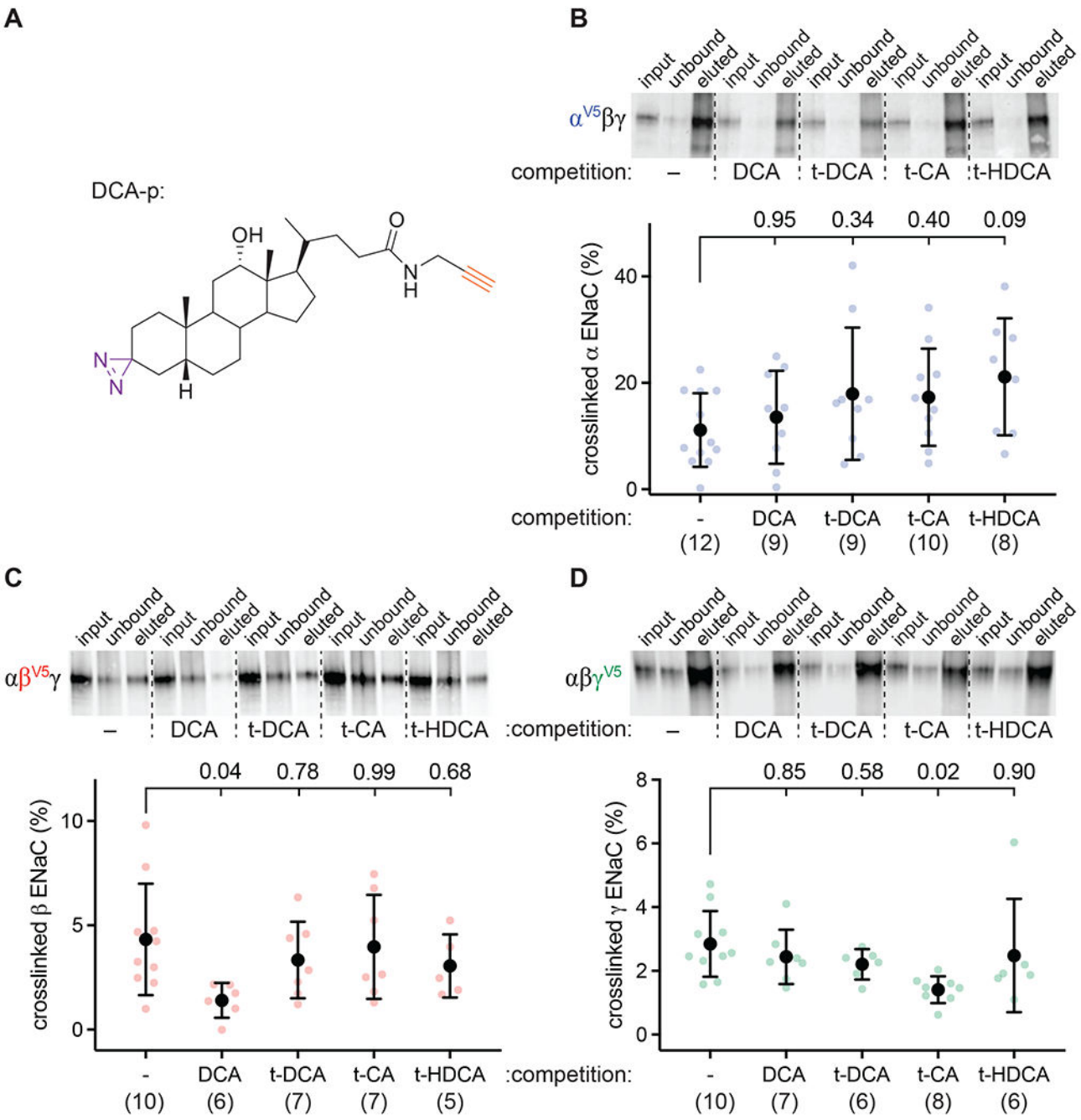

Figure 7. A bile acid derivative specifically crosslinks ENaC β and γ subunits.

A, Deoxycholic acid was derivatized (DCA-p) to include a photosensitive diazirine group (purple) and terminal alkyne group (orange) to facilitate conjugation to biotin. **B–D**, FRT cells expressing ENaC subunits with a single subunit bearing a C-terminal V5-epitope tag were incubated with DCA-p (50 μM) alone (−), or along with a competing bile acid (1 mM DCA, taurodeoxycholic acid (t-DCA), t-CA, or t-HDCA), as indicated. After UV light exposure, samples were processed to isolate probe-labeled proteins. Input, unbound and eluted fractions were subjected to SDS-PAGE and immunoblotted using anti-V5

antibodies. Quantified densities were used to calculate crosslinking efficiency, and the effect of competition on crosslinking efficiency was analyzed by 1-way ANOVA with Dunnett's post-hoc test. Individual data points (colored circles) and summary statistics (mean (SD)) are shown.

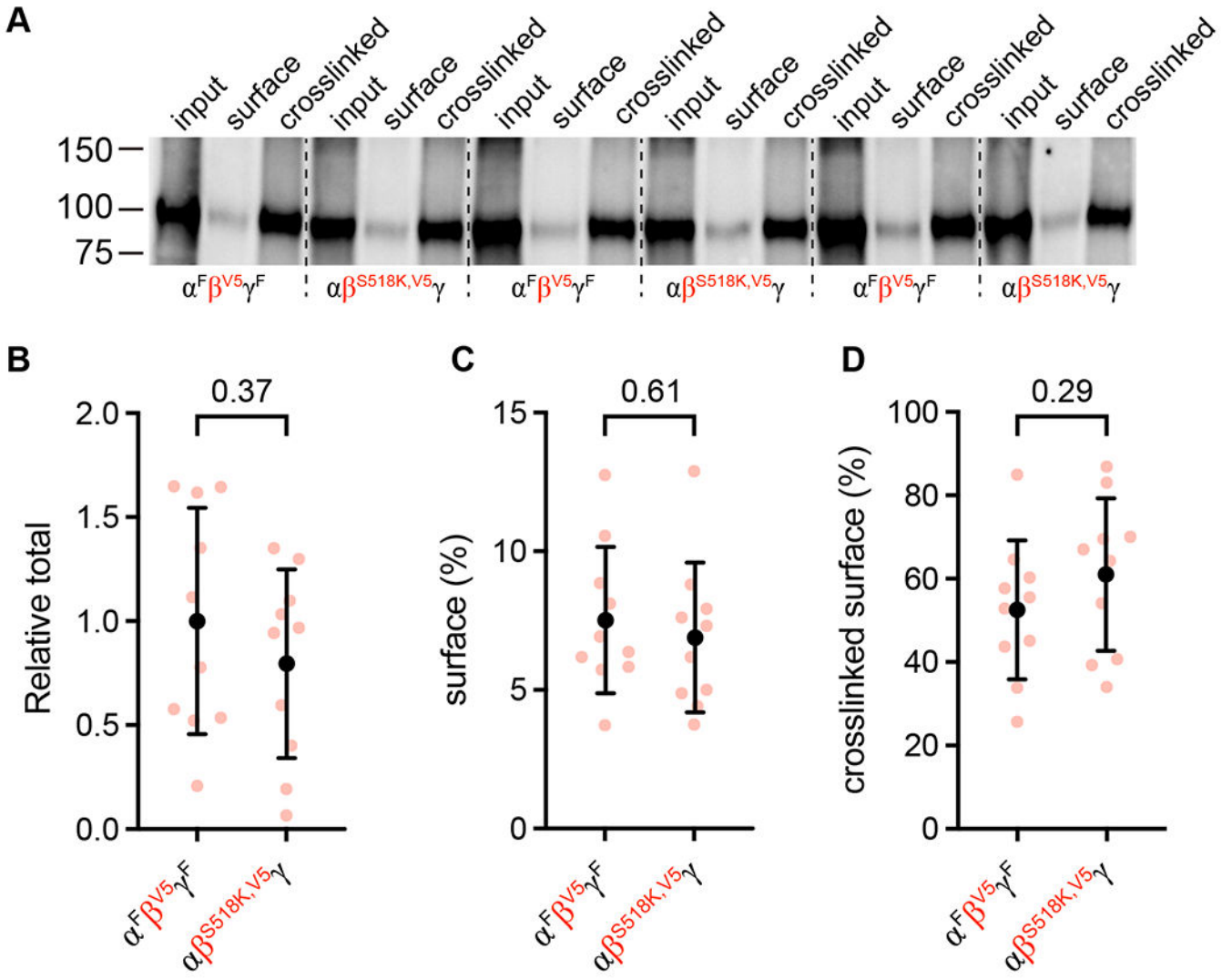

Figure 8. DCA-p crosslinking is similar in channels favoring open or closed states.

Channels with β subunit V5-epitope tags and with furin sites mutated ($\alpha^{F}\beta^{V5}\gamma^{F}$) to favor the closed state or with the degenerin site mutated ($\alpha\beta S518K^{V5}\gamma$) to favor the open state were expressed in FRT cells. Cells were incubated with 50 μM DCA-p, exposed to UV light, following which surface proteins were labeled using a cell-impermeant biotin reagent. Samples were processed to isolate probe-labeled proteins at the cell surface. Input, surface and crosslinked surface fractions were subjected to SDS-PAGE/blot with anti-V5. Top, representative blot. Bottom, Quantified band densities were used to calculate relative total expression (**B**), surface expression (**C**), and crosslinked surface proteins. Individual data points (colored circles) and summary statistics (mean (SD), $n = 10$ culture wells) for are shown. Data were compared by Student's t test.

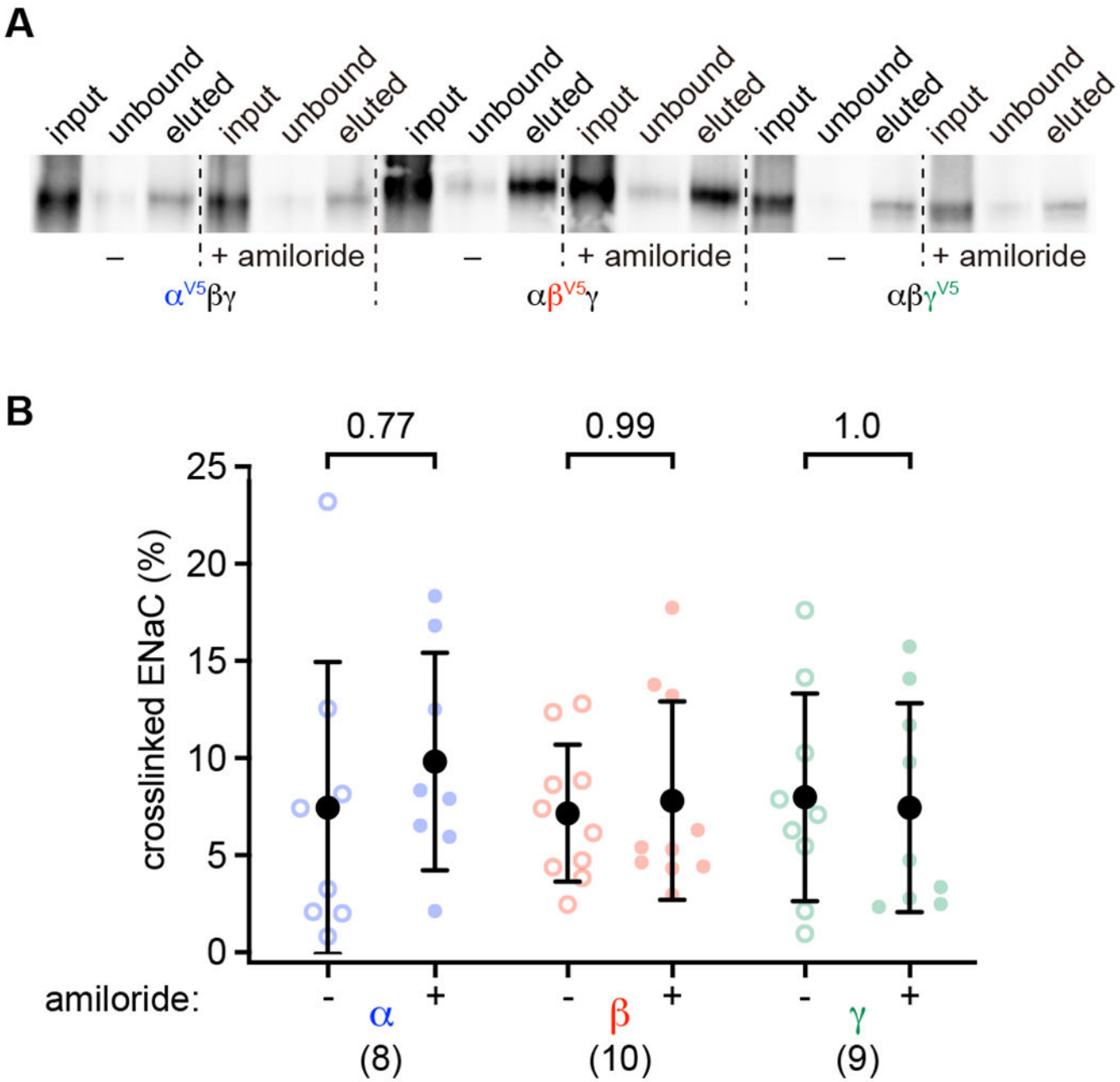

Figure 9. Amiloride does not reduce DCA-p crosslinking to ENaC.

FRT cells expressing ENaC subunits with a single subunit bearing a C-terminal V5 epitope tag were treated with 50 μM DCA-p ± 100 μM amiloride, exposed to UV light, and processed to isolate probe-labeled proteins. Input, unbound and eluted fractions were separated by SDS-PAGE followed by immunoblot with an anti-V5 antibody. **A**, Representative immunoblot. **B**, Quantified densities of input and eluted proteins were used to calculate the fraction of crosslinked ENaC. Individual data points (colored circles) and summary statistics (mean (SD)) are shown. The number of replicates (culture wells) are

indicated in parentheses. Data were analyzed by two-way ANOVA with Šidáks multiple comparison test.